ELSEVIER

Journal of Nuclear Materials 303 (2002) 226–239

journal of nuclear materials

www.elsevier.com/locate/jnucmat

Enthalpies of formation of Ce-pyrochlore, $Ca_{0.93}Ce_{1.00}Ti_{2.035}O_{7.00}$, U-pyrochlore, $Ca_{1.46}U^{4+}_{0.23}U^{6+}_{0.46}Ti_{1.85}O_{7.00}$ and Gd-pyrochlore, $Gd_2Ti_2O_7$: three materials relevant to the proposed waste form for excess weapons plutonium

K.B. Helean [a,*], A. Navrotsky [a], E.R. Vance [b], M.L. Carter [b], B. Ebbinghaus [c], O. Krikorian [c], J. Lian [d], L.M. Wang [d], J.G. Catalano [e]

[a] *Department of Chemical Engineering and Materials Science, Thermochemistry Facility, The University of California, Davis, CA 95616, USA*

[b] *Australian Nuclear Science and Technology Organization, Private Mailbag 1, Menai (Sydney), NSW 2234, Australia*

[c] *Lawrence Livermore National Laboratory, P.O. Box 808, Livermore, CA 94551, USA*

[d] *Department of Nuclear Engineering and Radiological Sciences, The University of Michigan, Ann Arbor, MI 48111, USA*

[e] *Department of Geological and Environmental Sciences, Stanford University, Palo Alto, CA 94305, USA*

Received 28 August 2001; accepted 18 January 2002

Abstract

High temperature oxide melt solution calorimetry was used to derive standard enthalpies of formation, ΔH^0_f (kJ/mol), for three pyrochlore phases: $Ca_{0.93}Ce_{1.00}Ti_{2.035}O_{7.00}$ (-3656.0 ± 5.6), $Ca_{1.46}U^{4+}_{0.23}U^{6+}_{0.46}Ti_{1.85}O_{7.00}$ (-3610.6 ± 4.1) and $Gd_2Ti_2O_7$ (-3822.5 ± 4.9). Enthalpy of drop solution data, ΔH_{ds}, were used to calculate enthalpies of formation with respect to an oxide phase assemblage, ΔH^0_{f-ox}: $CaO + MO_2 + 2TiO_2 = CaMTi_2O_7$ or $Gd_2O_3 + 2TiO_2 = Gd_2Ti_2O_7$, and an oxide/perovskite phase assemblage, $\Delta H^0_{f-pv+ox}$: $CaTiO_3 + MO_2 + TiO_2 = CaMTi_2O_7$, where M = Ce or U. All three pyrochlore samples were stable in enthalpy relative to an oxide assemblage with ΔH^0_{f-ox} (kJ/mol) ($Gd_2Ti_2O_7$) $= -113.4 \pm 2.8$; $\Delta H^0_{f-ox}(Ca_{1.46}U^{4+}_{0.23}U^{6+}_{0.46}Ti_{1.85}O_{7.00}) = -123.1 \pm 3.4$; $\Delta H^0_{f-ox}(Ca_{0.93}Ce_{1.00}Ti_{2.035}O_{7.00}) = -54.1 \pm 5.2$. U-pyrochlore was stable in enthalpy relative to an oxide/perovskite assemblage ($\Delta H^0_{f-pv+ox} = -5.1 \pm 4.0$ kJ/mol). Ce-pyrochlore was metastable in enthalpy relative to the oxide/perovskite phase assemblage ($\Delta H^0_{f-pv+ox} = +21.0 \pm 5.5$ kJ/mol). A significant metastability field was defined with respect to an oxide/perovskite phase assemblage. However, the proposed waste form baseline composition lies in the stable regions of the phase diagrams.

PACS: 65.50.+m; 61.16.Bg; 61.66.-f

1. Introduction

For the purpose of immobilizing excess weapons Pu, a crystalline ceramic waste form is being developed, which can be described as a pseudo-quaternary system consisting of $CaHfTi_2O_7$–$CaPuTi_2O_7$–$CaUTi_2O_7$–$Gd_2Ti_2O_7$ [1,2]. Three of the end-member phases, $CaPuTi_2O_7$, $CaUTi_2O_7$, and $Gd_2Ti_2O_7$ adopt the pyrochlore (Fd3m) structure. The other phase, $CaHfTi_2O_7$, 'hafnolite', is isostructural with $CaZrTi_2O_7$, zirconolite (C2/c). A necessary step toward optimizing processing conditions and assessing long-term chemical durability is determining the thermodynamic properties of the

* Corresponding author. Tel.: +1-530 754 2132; fax: +1-530 752 9703.

E-mail address: kbhelean@ucdavis.edu (K.B. Helean).

0022-3115/02/$ - see front matter
PII: S0022-3115(02)00795-X

waste form. The formation enthalpies of these phases are, therefore, of interest.

The thermodynamic properties of hafnolite and zirconolite were studied [3–5]. Enthalpies of formation, standard entropies and Gibbs energies have been derived using both high temperature oxide melt solution calorimetry for heats of formation as well as adiabatic calorimetric techniques for heat capacities (Table 1). These studies concluded that both hafnolite and zirconolite are stable with respect to their binary oxides as well as to a perovskite – binary oxide phase assemblage. The standard entropies were derived from adiabatic C_p data. They lie between values for the stoichiometric sum of the standard entropies of their component oxides (derived by the Neumann–Kopp rule) and values for a mixture of $CaTiO_3$ and binary oxides [6]. This suggests that, in the absence of adiabatic C_p data, an adequate estimate of entropy may be obtained by taking the average of these two summations. A similar study of the pyrochlore end-members is necessary in assessing the thermodynamic stability of the proposed waste form.

Cerium has been commonly used as a surrogate for Pu in solid-state studies owing to their similar ionic radii ($Ce^{4+} = 0.097$ nm and $Pu^{4+} = 0.096$ nm for CN = 8) [7]. The compound $CaCeTi_2O_7$ is isostructural with $CaPuTi_2O_7$, adopting the pyrochlore structure (Fd3m) [8]. The physical and chemical properties of cerium pyrochlore and the related zirconolite (C2/c), nominally $CaZr_{0.8}Ce_{0.2}Ti_2O_7$, as well as zirconolite compositions doped with other actinides and REE, have been rigorously studied in an effort to estimate the corresponding properties of the Pu host materials [9–28]. In this study a similar strategy was employed. A calorimetric study of $CaCeTi_2O_7$ was undertaken in order to estimate the thermodynamic properties of $CaPuTi_2O_7$.

Recently Xu and Wang [29], estimated the formation energetics of zirconolite/pyrochlore phases, $CaMTi_2O_7$, where M = Zr, Hf, Ce, Th, U, Np, Pu, Am, Po, using a linear free energy model similar to that of Sverjensky and Molling [30]. This model is analogous to the Hammett linear free energy relationship for aqueous organic reactions [31]. Their model assumes a linear correlation between the standard Gibbs energy of formation of the end-member solid and the standard Gibbs energy of formation of the aqueous tetravalent cation M^{4+} within an isostructural family. Xu and Wang predicted Gibbs energy of formation for reactions (1)–(3) of −7.66, −4.56 and −10.42 kJ/mol respectively.

$$CeO_2 + CaTiO_3(\text{perovskite}) + TiO_2(\text{rutile}) = CaCeTi_2O_7(\text{pyrochlore}), \quad (1)$$

$$UO_2 + CaTiO_3(\text{perovskite}) + TiO_2(\text{rutile}) = CaUTi_2O_7(\text{pyrochlore}), \quad (2)$$

$$PuO_2 + CaTiO_3(\text{perovskite}) + TiO_2(\text{rutile}) = CaPuTi_2O_7(\text{pyrochlore}). \quad (3)$$

Due to the lack of measured data, in order to derive the Gibbs energy relation for pyrochlore, Xu and Wang assumed that the energetic difference between zirconolite and pyrochlore phases of the same composition is small (1.3 kJ/mol). This assumption is based on observations that pyrochlore lamellae are observed in synthetic zirconolite [32]. They then used the zirconolite and hafnolite data reported in Table 1 to fit a pyrochlore curve. Assessing the uncertainties in their model is difficult. Therefore, the experimental determination of the formation energetics of these pyrochlore phases is needed.

The objective of this study is to determine experimentally the enthalpies of formation of three pyrochlore phases relevant to the waste form: $CaCeTi_2O_7$ (as

Table 1
Enthalpy, entropy and Gibbs energy of formation from the elements, oxides and a perovskite + oxide assemblage for $CaZrTi_2O_7$ and $CaHfTi_2O_7$ [2–5]

	ΔH_f^0 (kJ/mol)	S^0 (J/mol K)	ΔG_f^0 (kJ/mol)
$CaZrTi_2O_7$	-3713.7 ± 4.5	193.3	-3514.5 ± 4.5
$CaHfTi_2O_7$	-3779.4 ± 4.7	194.4	-3579.2 ± 4.7
	ΔH_{f-ox}^0 (kJ/mol)[a]	ΣS_{f-ox}^0 (J/mol K)	ΔG_{f-ox}^0 (kJ/mol)
$CaZrTi_2O_7$	−88.6	189.2	−89.3
$CaHfTi_2O_7$	−110.1	198.1	−108.5
	$\Delta H_{f-pv+ox}^0$ (kJ/mol)[b]	$\Sigma S_{f-pv+ox}^0$ (J/mol K)	$\Delta G_{f-pv+ox}^0$ (kJ/mol)
$CaZrTi_2O_7$	−7.8	194.3	−7.0
$CaHfTi_2O_7$	−29.3	203.3	−26.2

[a] $CaO + MO_2 + 2TiO_2 = CaMTi_2O_7$.
[b] $CaTiO_3 + MO_2 + TiO_2 = CaMTi_2O_7$, where M = Zr, Hf.

an analogue to $CaPuTi_2O_7$), $CaUTi_2O_7$, and $Gd_2Ti_2O_7$. Due to their refractory nature, high temperature oxide melt drop solution calorimetric techniques were used [33,34]. An assessment of waste form stability is offered.

2. Sample synthesis

Cerium pyrochlore, nominally $CaCeTi_2O_7$, was synthesized at the Australian Nuclear Science and Technology Organization (ANSTO) by shear-mixing tetraisopropyl titanate, $Ti(OC_3H_7)_4$, with an aqueous solution of Ca and Ce^{3+} nitrates. The target cation ratio was 0.9Ca:1.0Ce:2.0Ti. The reduction of Ca was necessary to eliminate $CaTiO_3$ as an impurity. The mixture was stir-dried and calcined at 750 °C to produce a quasi-amorphous oxide material. Pellets were fired in air at 1200 °C for 96 h. Lower firing temperatures resulted in an incomplete reaction and higher temperatures resulted in Ce reduction, thus reducing pyrochlore yields. The Gd-pyrochlore sample, $Gd_2Ti_2O_7$, was provided by Lawrence Livermore National Laboratory (LLNL). The sample was synthesized by ball milling stoichiometric portions of reagent grade binary oxides, pressing the mixture into pellets and firing at 1500 °C for 120 h. The target cation ratio was 1Gd:1Ti. The U-pyrochlore sample (P249), nominally $CaUTi_2O_7$, was provided by LLNL. The sample was synthesized using a mixture of reagent grade $Ca(OH)_2$, UO_2 and TiO_2, anatase with excess Ca and Ti in the ratio 2.1Ca:1.0U:3.7Ti. This starting mixture was found to maximize U-pyrochlore yields. The powder mixture was ball milled for 1 h in the presence of water and then dried in an oven. The powder was then calcined in stagnant air in a rotary kiln at 750 °C for 1 h. Several 1/2 in. diameter pellets were pressed at 18,000 psi. These pellets were then placed on platinum foil in an alumina dish and heated to 1350 °C for 4 h in a flowing argon atmosphere.

3. Analytical methods

3.1. X-ray powder diffraction

XRD data for the Ce-pyrochlore sample were collected at the National Synchrotron Light Source (NSLS) at Brookhaven National Laboratory ($\lambda = 0.07076$ nm) using a GE111-position sensitive detector. Rietveld analysis was conducted using the General Structure Analysis System (GSAS) [35]. XRD data for the Gd- and U-pyrochlore samples were collected on a Scintag PADV using a Cu anode, a tube voltage of 45 kV, over an angular range of 14–94° 2θ with a step size of 0.02° and a 5 s dwell time. Rietveld analysis of the U-pyrochlore sample was performed using the RIQAS software from Materials Data, Inc. [36].

3.2. Electron microprobe analysis

Quantitative chemical analyses of the Ce- and Gd-pyrochlore samples were conducted using a Cameca SX50 electron microprobe (EMPA) with wavelength dispersive spectrometry (WDS), an accelerating voltage of 20 kV, a probe current of 10 nA and a spot size of 1 μm. Quantitative WDS of the U-pyrochlore samples was conducted using a lower accelerating voltage of 15 kV.

3.3. High-resolution transmission electron microscopy

High-resolution transmission electron microscopy (HRTEM) was used to assess the homogeneity of the pyrochlore sample on a nano-scale. Because previous reports indicated that pyrochlore lamellae are commonly found in zirconolite, verification that our sample did not contain such exsolution features was deemed necessary. TEM micrographs were collected using a JEOL 2010F electron microscope with a field emission source. The accelerating voltage was 200 kV. Both bright-field and high-resolution imaging were used to characterize the nano-structure of the sample. Powder samples were prepared by grinding under methanol and suspending small particles on holey carbon grids.

3.4. Extended X-ray absorption fine structure and X-ray absorption near edge structure spectroscopic analysis

U L_{III}-edge X-ray absorption near edge structure (XANES) and extended X-ray absorption fine structure (EXAFS) spectroscopy were used to evaluate the oxidation state of U in P249. EXAFS and XANES measurements were carried out at the Stanford Synchrotron Radiation Laboratory on wiggler beamline 4-3 using Si(2 2 0) monochromator crystals in the $\phi = 0°$ orientation. Data were collected in transmission mode at room temperature with the sample perpendicular to the beam. Energy was calibrated using a Y-metal foil; the first inflection points of the Y K-absorption edge was set at 17,038 eV. Data were processed using EXAFSPAK [37]. EXAFS data were background subtracted and k^3-weighted, then fit using scattering path phase and amplitude functions generated by FEFF 7.0 [38].

4. Sample characterization

4.1. Ce-pyrochlore

The lattice parameter, a, for cerium pyrochlore was 1.01477(3) nm as determined by Rietveld analysis of synchrotron data. This matched well with the reported value of 1.0142 nm [39]. The weight fraction pyrochlore in the ANSTO sample was 0.943 with the major

impurity, CeO_2, comprising 0.057 weight fraction. The $CaTiO_3$ impurity was not refined in the analysis due to its minor occurrence and significant peak overlap with CeO_2. The perovskite impurity content was estimated from back-scattered electron (BSE) images as approximately 0.01 volume fraction. These analyses correspond to 97.48 mol% Ce-pyrochlore + 2.16 mol% CeO_2 + 0.36 mol% perovskite in the ANSTO sample. Significant peak overlaps and low peak intensities for the CeO_2 and $CaTiO_3$ phase precluded the determination of their lattice parameters by XRD.

The Ce-pyrochlore sample was analyzed by EMPA-WDS using the following standards, $CaSiO_3$, wollastonite, CeO_2, cerianite and TiO_2, rutile. Oxygen was determined by stoichiometry (Table 2). The measured CeO_2 and TiO_2 contents are, within error, equal to the theoretical elemental weight percent values. The measured CaO content (wt%) is significantly less than the theoretical value. The ideal pyrochlore structure contains four cation sites. Normalizing the data to four cations results in excess oxygen, i.e. greater then seven oxygen atoms per formula unit. Excess oxygen is unlikely. Therefore, the data were normalized to seven oxygen atoms. The calculated stoichiometry reveals a 0.07 mol Ca deficiency that is balanced by 0.035 mol excess Ti plus 0.035 mol Ca^{2+} vacancies. Vacancies of this type are well documented in the pyrochlore structure [9]. The calculated stoichiometry is $Ca_{0.93}Ce_{1.00}Ti_{2.035}O_{7.00}$.

Table 2
Results of the EMPA-WDS analysis for the pyrochlore samples[a]

	Measured composition	Nominal composition	Composition normal to seven oxygens
Ce-pyrochlore			
O	28.58 ± 0.36	28.87	7.000
Ca	9.50 ± 0.17	10.33	0.932
Ti	24.87 ± 0.33	24.68	2.035
Ce	35.79 ± 0.51	36.12	0.999
Total	98.73 ± 1.22 (19)	100.00	
Gd-pyrochlore			
O	20.86 ± 0.16	21.44	7.000
Ti	17.91 ± 0.24	18.34	1.998
Gd	58.23 ± 0.47	60.22	2.002
Total	96.99 ± 0.64 (15)	100.00	
U-pyrochlore			
O	23.17 ± 0.51	23.05	7.000
Ca	12.83 ± 0.28	8.25	1.460
Ti	20.76 ± 0.47	19.71	1.850
U	36.34 ± 0.96	48.99	0.690
Total	93.10 ± 1.46 (19)	100.00	

[a] Data are reported as weight percent element. Oxygen is calculated from stoichiometry. Number of analyses in parentheses. Averages of measured and normalized data are reported. Errors are 2σ.

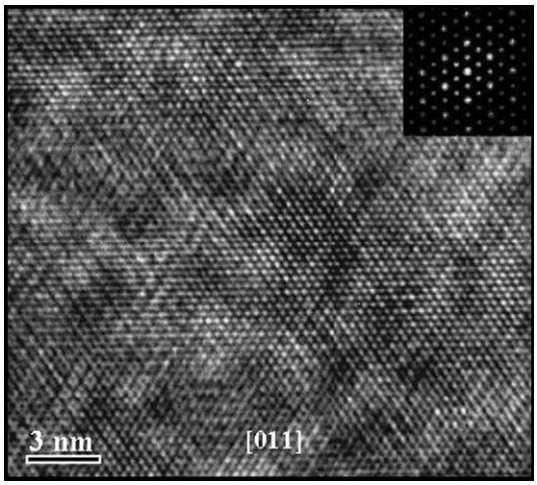

Fig. 1. HRTEM micrograph of Ce-pyrochlore down the [0 1 1] zone axis.The sample is homogeneous pyrochlore. No exsolution features are observed.

Two impurities were observed in BSE images, $CaTiO_3$, perovskite, and CeO_2, cerianite. Due to their small grain size (<1 μm) no quantitative determination of the chemistry of the two impurities was possible using EMPA.

HRTEM micrographs indicated that the Ce-pyrochlore sample was homogeneous pyrochlore (Fig. 1). No exsolved zirconolite was observed. All grains analyzed were pyrochlore as determined by selected area electron diffraction (SAED). The cerianite and perovskite impurities were not observed in bright-field images due to their low occurrence (<3 mol% combined impurities).

The Ce-pyrochlore sample provided by ANSTO for this study contains minor amounts of two impurities: CeO_2 (2.16 mol%) and $CaTiO_3$ (0.36 mol%). The stoichiometry calculated from EMPA results is $Ca_{0.93}Ce_{1.00}Ti_{2.035}O_{7.00}$. No exsolution features were observed in HRTEM images. Both the CeO_2 and $CaTiO_3$ impurities are assumed to be stoichiometric for the purpose of correcting the calorimetric data.

4.2. Gd-pyrochlore

Only pyrochlore peaks were observed in the XRD pattern for $Gd_2Ti_2O_7$. A least squares refinement of the data using Si as an internal standard gave the lattice parameter, a, as 1.0186(5) nm which is, within error, equal to the reference value of 1.0185 nm [40].

The Gd-pyrochlore sample was analyzed using Gd–Ga garnet, and TiO_2, rutile as standards. Oxygen content was determined by stoichiometry. All of the

analytical totals were low ($96.99 \pm 0.64\%$) (Table 2). This is attributed to the fine particle size and surface roughness of the powdered sample [41]. Considering the normalized data, the Gd-pyrochlore is stoichiometric, $Gd_2Ti_2O_7$, within the error of the analysis. BSE images revealed a small impurity, <0.01 volume fraction, TiO_2. Using the calculated density of the Gd-pyrochlore (6.565 g/cm^3) and the theoretical density of rutile (4.25 g/cm^3) [42], the volume fractions were converted to mole fractions. The sample contains 0.999 mol fraction Gd-pyrochlore + 0.001 mole fraction TiO_2.

Numerous HRTEM studies of $Gd_2Ti_2O_7$ were recently reported [43–46]. All of these studies indicated that Gd-titanate pyrochlore is homogeneous on a nano-scale. Because this pyrochlore does not contain two different large cations, it cannot adopt the zirconolite-type structure. As a result exsolved zirconolite was not expected. Sample preparation and instrumental parameters were the same as for Ce-pyrochlore. HRTEM images of the LLNL Gd-pyrochlore sample indicated that this sample was also homogeneous on a nano-scale (Fig. 2). HRTEM confirmed that the sample was homogeneous pyrochlore and no impurities or abnormalities were observed.

The Gd-pyrochlore sample provided by LLNL for this study contains one minor impurity: TiO_2 (0.01 mol%). The sample is stoichometric $Gd_2Ti_2O_7$ calculated using normalized EMPA results. No exsolution features were observed in HRTEM images. Because the TiO_2 impurity is present in an amount too small to be significant to the calorimetric measurements, the data are corrected assuming that $Gd_2Ti_2O_7$ is phase pure.

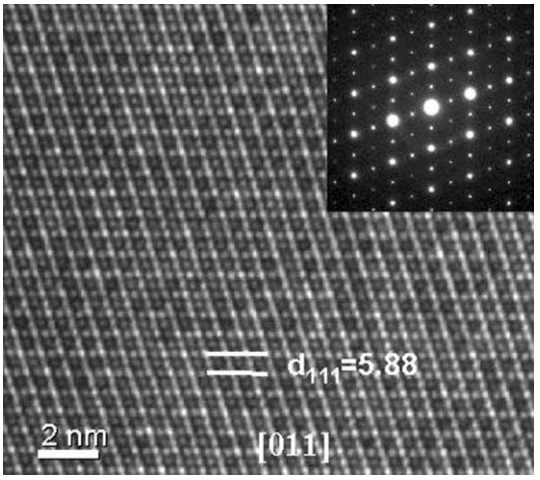

Fig. 2. HRTEM micrograph of $Gd_2Ti_2O_7$ down the [0 1 1] zone axis. The measured *d*-spacing of the 111 planes is 5.88 Å. The calculated lattice parameter, *a*, is 10.184 Å. This is in reasonable agreement with data from refinement of XRD data (a = 10.186(5) Å).

4.3. U-pyrochlore

Rietveld analysis of XRD data indicated that P249 consisted of 86.31 wt% U-pyrochlore plus 13.69 wt% rutile. Using the calculated densities for both phases, (U-pyrochlore, $\delta = 5.3393$ g/cm^3; rutile, $\delta = 4.3553$ g/cm^3) the mole fractions were calculated as 0.5813 U-pyrochlore and 0.4187 TiO_2, rutile. The refined lattice parameter for the U-pyrochlore was 1.01775(1) nm and for the rutile phase $a = 0.45901(2)$ and $c = 0.29564(5)$ nm.

P249 was analyzed by EMPA-WDS using $CaSiO_3$, wollastonite, TiO_2, rutile, and UO_2, uraninite, as standards. Oxygen was calculated by stoichiometry assuming all the uranium is tetravalent (Table 2). All analytical totals were low ($93.85 \pm 1.60\%$). This is attributed to the fine particle nature and surface roughness of the powder sample [41]. A comparison of the normalized elemental data to the calculated values indicates that the U and Ti-content is significantly lower than predicted by ideal stoichiometry. In addition, the Ca element percent value is significantly higher than the calculated values. Normalizing the data to four cations, the calculated stoichiometry of the U-pyrochlore phase based on EMPA is $Ca_{1.46}U_{0.69}Ti_{1.85}O_{6.54}$. The rutile phase has a calculated stoichiometry based on EMPA of $Ti_{0.97}U_{0.01}Ca_{0.02}O_{1.983}$. On the basis of the microprobe analysis, the U-pyrochlore sample is non-stoichiometric with excess Ca, a deficiency in Ti and significant (0.46 mol per formula unit) oxygen vacancies.

The calculated stoichiometry indicates that a significant amount of U is present on the Ti-site, approximately 0.15 mol per formula unit. U^{4+} is much larger that Ti^{4+}, therefore such a substitution would induce significant strain in the crystal structure. Because the crystallographic sites for Ti^{4+} in both perovskite and pyrochlore are similar, i.e. Ti^{4+} is octahedrally coordinated and the octahedra share corners, the U^{4+}–Ti^{4+} substitution measured for perovskite may be used to estimate that substitution limit for pyrochlore. The presence of U^{4+} in perovskite has been reported, with up to 0.1 mol U^{4+} substituting on the Ca^{2+} site [24]. There was no evidence that U^{4+} substituted for Ti^{4+} on octahedral sites. This suggests that the substitution of U^{4+} for Ti^{4+} in perovskite may not be possible. The EMPA indicates that the pyrochlore has 0.15 mol U^{4+} per formula unit substituting for Ti^{4+}. This may be due to a greater U^{4+} capacity of the Ti-site in pyrochlore or it may be due to the presence of uranium in a higher oxidation state, see below, which would decrease its radius.

The XANES spectrum of P249 was compared to $UO_{2.08}$ (a U^{4+} standard) and γ-UO_3 (a U^{6+} standard) to evaluate the oxidation state of U in the sample (Fig. 3). The $UO_{2.08}$ and γ-UO_3 spectra are consistent with published spectra of UO_{2+x} ($x \leqslant 0.1$) [47], and UO_3 [48]. The shoulder on the high-energy side of the main absorption

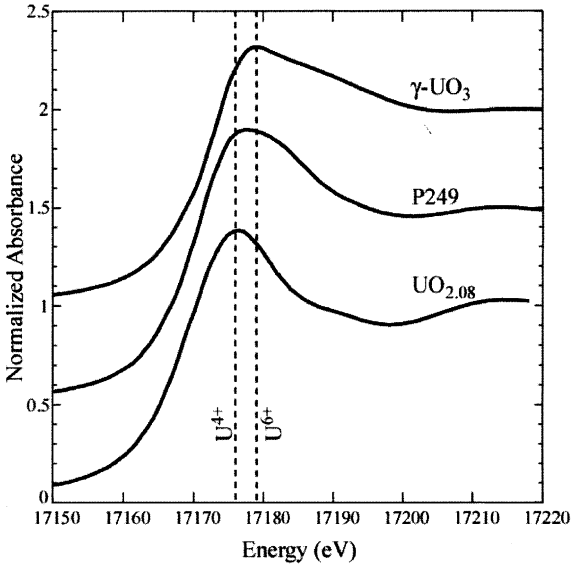

Fig. 3. The XANES spectra of the U-samples. The absorption edge position for sample P249 indicated a mixture of U^{4+} and either U^{5+} or U^{6+}, or both.

edge of γ-UO_3, occurring at ≈17 190 eV, is a multiple-scattering resonance feature characteristic of the axial oxygen atoms from an uranyl (UO_2^{2+}) group [47]. The XANES spectrum of the P249 sample shows significant broadening of the main edge. While the resonance feature characteristic of a uranyl group is not present, the edge broadening is indicative of a mixed U valence. Main edge broadening has been observed in other mixed-valence U compounds, including U_3O_8 [48,49].

The EXAFS spectra and best-fit for sample P249 are shown in Fig. 4. Phase and amplitude functions were calculated using FEFF 7.0 [38] based on the crystal structure obtained through Rietveld refinement of X-ray powder diffraction data. The first five single-scattering paths, corresponding to the five closest neighboring atoms, were fit to the data. Their relative contributions were based on the site occupancies provided by the crystal structure data. Attempts were made to fit a U–O scattering pathway of length ≈1.80 Å, corresponding to scattering from the axial oxygen of a uranyl moiety. This could not be fit to the data. The EXAFS thus does not support the presence of uranyl groups, and is consistent with the crystal structure derived from Rietveld refinement of powder diffraction data.

The XANES spectrum for P249 indicates a mixed oxidation state of U in the sample. While the EXAFS data rule out the presence of uranyl groups, as does the lack of a resonance feature at ≈17 190 eV in the XANES spectrum, U^{6+} may occur in a non-uranyl coordination (no axial oxygen atoms). The combined XANES and EXAFS data suggest the U-pyrochlore contains a mixture of U^{4+} and either U^{5+} or U^{6+}.

In light of the XANES/EXAFS results, the EMPA results were adjusted to reflect the presence of hexavalent uranium. Normalizing the data to seven oxygens per formula unit gives a calculated sotichiometry of $Ca_{1.46}U^{4+}_{0.23}U^{6+}_{0.46}Ti_{1.85}O_{7.00}$. This new formula is consistent with the qualitative interpretation of the XANES and EXAFS data. This formula is used in the thermodynamic analysis.

Because EMPA indicated that the U-pyrochlore sample was non-stoichiometric and possibly had a large (0.15 per formula unit) substitution of U for Ti, a HRTEM study of the nano-structure of the sample was conducted. HRTEM micrographs indicated that the sample consisted of homogeneous pyrochlore plus rutile (Fig. 5). No intergrown phases or exsolution features were observed. No superlattice reflections were observed in the SAED patterns. However, the superlattice is

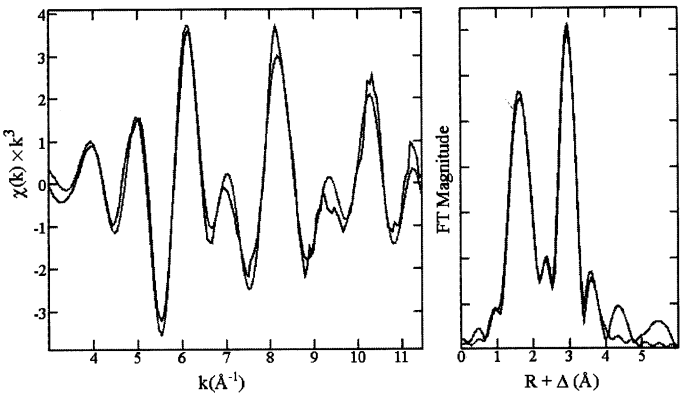

Fig. 4. EXAFS data (solid line) and best fit (dotted line) for the first five coordination shells for P249. The EXAFS data did not indicate the presence of uranyl groups. However, U^{6+} may be present in a non-uranyl coordination.

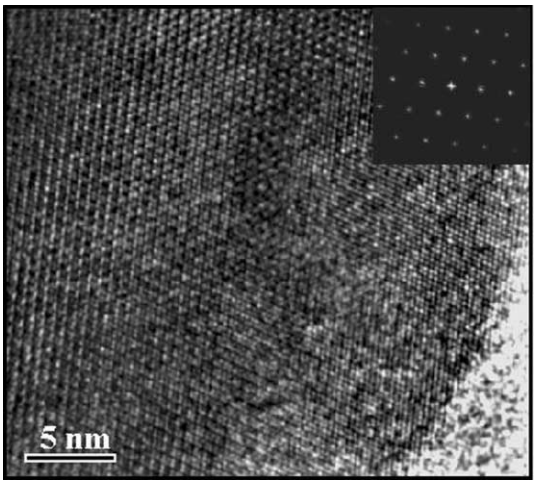

Fig. 5. HRTEM micrograph of U-pyrochlore down the [0 1 1] zone axis. The superlattice is apparent in the micrograph, but fails to show up in the SAED pattern (inset). This is due to the thinning of the grain. Note the disappearance of the super lattice from micrograph near the grain edge. The sample is homogeneous pyrochlore with no exsolved zirconolite observed.

apparent in the HRTEM image. As the grain thins at its edge, the superlattice fringes disappear resulting in an image best represented by a fluorite structure.

The P249 sample provided by LLNL contains two phases, a non-stoichiometric U-pyrochlore (58.13 mol%) and a non-stoichiometric rutile (41.87 mol%). The results of a XANES/EXAFS study of P249, indicated that the sample contains multi-valent uranium with spectroscopic features consistent with U_3O_8. Recalculating the EMPA results assuming enough hexavalent uranium to bring the oxygen total to seven results in the following stoichiometry: $Ca_{1.46}U^{4+}_{0.23}U^{6+}_{0.46}Ti_{1.85}O_{7.00}$. The U^{6+}/U^{4+} ratio is two and is identical to the U^{6+}/U^{4+} ratio in U_3O_8. The presence of U^{5+} can not be ruled out. Recent investigations into the valence state of uranium in zirconolite revealed the presence of U^{4+} and U^{5+}, but no U^{6+} (ANSTO, unpublished data). However, in a thermodynamic cycle the enthalpy contribution from U^{5+} is equivalent to the enthalpy contributions of $0.5U^{4+} + 0.5U^{6+}$. Therefore, our estimated stoichiometry for the P249 pyrochlore is deemed valid and used in all thermodynamic calculations. The measured stoichiometry for the rutile phase, $Ti_{0.97}U_{0.01}Ca_{0.02}O_{1.983}$, indicates that U and Ca are present in small (0.03 mol per formula unit) amounts. Such substitutions are unlikely and these EMPA results may reflect the contribution from neighboring grains of pyrochlore. The lattice parameters derived for the P249 rutile phase by Reitveld refinement are identical to those reported for pure stoichiometric rutile [41]. Therefore, for the purpose of correcting the thermodynamic cycles for sample P249, the rutile phase is considered to be stoichiometric TiO_2.

5. Calorimetric methods

High temperature oxide melt solution calorimetry was used to measure drop solution enthalpies of the pyrochlore samples plus their binary oxide components. A Tian-Calvet twin microcalorimeter was used to collect drop solution data. The details of the calorimeter design and operation are described in detail elsewhere [33,34]. Prior to calorimetry, the powder samples were dried at 700 °C for a minimum of 1 h. The single exception to this was the $UO_{2.08}$ sample that was dried at 200 °C for 1/2 h to avoid further oxidation of the uranium. The solvent used in this study was sodium molybdate, $3Na_2O \cdot 4MoO_3$, at 976 K. Drop solution enthalpies, ΔH_{ds} were measured by dropping pellets (≈5 mg) of the powder sample from room temperature into the solvent at calorimeter temperature. Thus, these measurements consist of two components, the heat content of the sample, $\int_{298}^{T} C_p \, dT$, and the heat of solution, ΔH_s Oxygen was bubbled through the melt to aid in the dissolution of the pellets and to provide high oxygen fugacity that ensured the oxidation of U^{4+} to U^{6+} [50]. The calorimeters were calibrated using the heat content of α-Al_2O_3 [51]. The measured values of drop solution were used in the appropriate thermodynamic cycles to calculate the enthalpies of formation from the oxides. Reference data for the enthalpies of formation from the elements for the binary oxides were used to calculate the enthalpies of formation from the elements for the compounds [52].

6. Results

6.1. Calorimetric data: Ce-pyrochlore

Drop solution experiments using $3Na_2O \cdot 4MoO_3$ solvent at 976 K were carried out for $CaCO_3$, calcite, TiO_2, rutile, CeO_2, cerianite, $CaTiO_3$, perovskite and the Ce-pyrochlore sample (Table 3). The ΔH_{ds} value for the Ce-pyrochlore was corrected for the cerianite and perovskite impurities through a thermodynamic cycle assuming a mechanical mixture of 0.9748 Ce-pyrochlore + 0.0216 perovskite + 0.0036 cerianite (Table 4). The relative error for the ΔH_{ds} value for Ce-pyrochlore was larger than the relative errors for the other materials by approximately 0.5 percent. This was consistent with the sample heterogeneity, which was expected to increase the scatter in the data.

The ΔH_{ds} value for TiO_2 is consistent with previously reported data. Prior experiments collected solution enthalpies, ΔH_s by equilibrating the TiO_2 samples at calorimeter temperature before stirring the powder into the melt. In order to compare ΔH_{ds} to ΔH_s for TiO_2, the calculated heat content (48.9 kJ/mol) is subtracted such that $\Delta H_s = \Delta H_{ds} - \int_{298}^{976} C_p(TiO_2 \, dT)$. The resulting value of 10.02 ± 0.82 kJ/mol falls within the range of the

Table 3
Drop solution enthalpies used in thermodynamic cross checks and the calculation of formation enthalpies[a]

Material	ΔH_{ds} (kJ/mol)
Ce-pyrochlore	160.72 ± 4.48 (12)
Gd-pyrochlore	82.71 ± 2.11 (12)
U-pyrochlore (P249)	66.85 ± 1.83 (11)
TiO_2, rutile	58.92 ± 0.82 (16)
$CaCO_3$	119.70 ± 1.02 (7)
$CaTiO_3$	53.94 ± 0.64 (3)
CeO_2	73.39 ± 1.65 (10)
Gd_2O_3	-148.54 ± 1.60 (10)
$UO_{2.08}$	-124.63 ± 2.30 (11)
γ-UO_3	9.49 ± 1.53 (2)
CaO (calculated)	-90.70 ± 1.69 (7)

[a] Errors are calculated as two standard deviations of the mean. Number of experiments is in parentheses. Data were collected using sodium molybdate ($3Na_2O \cdot 4MoO_3$) solvent at 976 K.

previously reported data which spanned from 9.96 to 10.33 kJ/mol [53,54].

The ΔH_{ds} of $CaCO_3$ was measured to obtain ΔH_{ds} CaO because CaO is unstable under ambient conditions (Table 4). No previous reports of ΔH_{ds} of $CaCO_3$ or ΔH_s of CaO using $3Na_2O \cdot 4MoO_3$ solvent were available for comparison. Likewise, there are no previously published values to compare ΔH_{ds} of CeO_2.

6.2. Thermodynamic cycle: Ce-pyrochlore

The calorimetric data were used in a thermodynamic cycle to calculate the enthalpy of formation, ΔH_f^0 from the oxides (Table 4). Using reference data for the standard enthalpies of formation from the elements for the binary oxides, the ΔH_f^0 for Ce-pyrochlore was derived, $\Delta H_f^0 = -3656.0 \pm 5.6$ kJ/mol (Table 4). Ce-pyrochlore is stable with respect to the oxides at 298 K with $\Delta H_{f-ox}^0 = -54.1 \pm 5.2$ kJ/mol. However, when the stability of Ce-pyrochlore is assessed with respect to a perovskite phase assemblage (Table 4), it is metastable by +21 kJ/mol. This is consistent with reports that synthesis of phase pure Ce-pyrochlore is difficult and always results in the formation of some perovskite, $CaTiO_3$ [55]. The observation that the pyrochlore formed deviates from the ideal $CaCeTi_2O_7$ stoichiometry also supports limited stability; the non-stoichiometric variant may be stabilized by configurational entropy.

6.3. Calorimetric data and thermodynamic cycle: Gd-pyrochlore

Drop solution experiments were carried out for Gd_2O_3 and $Gd_2Ti_2O_7$ using $3Na_2O \cdot 4MoO_3$ at 976 K (Table 3). The ΔH_{ds} value for Gd_2O_3 was previously published and was shown to be consistent with observed lanthanide enthalpy trends [56]. These data along with the ΔH_{ds} for TiO_2 reported in Table 3 were used in a thermodynamic cycle to calculate ΔH_{f-ox}^0 for $Gd_2Ti_2O_7$ (Table 4). Gd-titanate pyrochlore is energetically stable with respect to the oxides by -113.4 ± 2.8 kJ/mol. Using reference data for the standard enthalpies of formation from the elements for the binary oxides, the ΔH_f^0 for Gd-titanate pyrochlore was derived, $\Delta H_f^0 = -3822.5 \pm 4.9$ kJ/mol (Table 4).

6.4. Calorimetric data: U-pyrochlore

Drop solution experiments were carried out for $UO_{2.08}$, γ-UO_3 and the P249 sample using $3Na_2O \cdot 4MoO_3$ at 976 K (Table 3). The ΔH_{ds} value for P249 was corrected for the presence of 0.423 mole fraction TiO_2, rutile, assuming a mechanical mixture (Table 4). The $UO_{2.08}$ sample gave a large exothermic signal with $\Delta H_{ds} = -124.6 \pm 2.3$ kJ/mol. The large exothermic ΔH_{ds} for $UO_{2.08}$ plus a solvent color change from white to yellow were indicators of U oxidation during dissolution. The γ-UO_3 gave a very small heat signal. As a result only two of the five experiments had less than 5% relative baseline contributions and were used in further calculations. The typical approach for collecting calorimetric data on samples with small ΔH_{ds} is to use a solution calorimetric technique that requires the sample to be equilibrated at calorimeter temperature before lowering into the solvent for dissolution. This increases the total signal by eliminating the endothermic contribution from the heat content, $\int_{298}^{975} C_p \, dT$, of the sample. This approach is not possible with γ-UO_3 as it does not persist at calorimeter temperature.

6.5. Thermodynamic cycles: U-pyrochlore

The ΔH_{ds} for $UO_{2.08}$ was corrected for the presence of a higher uranium oxidation state, formally taken as 0.08 mol per formula unit of hexavalent uranium (Table 4). The calculated ΔH_{ds} value for stoichiometric UO_2 is -136.4 ± 2.3 kJ/mol. In order to test the accuracy of the uranium drop solution data as well as to verify the final U oxidation state in the solvent, reference data for UO_2 and γ-UO_3 were compared to the measured data (Table 4). The calculated enthalpy of oxidation of UO_2 to γ-UO_3 using measured data was -135.9 ± 2.8 kJ/mol. This is within error equal to the value calculated from reference data, -138.9 ± 1.3 kJ/mol. Therefore, the ΔH_{ds} values for UO_2 and γ-UO_3 are accurate and the final state of the uranium in the $3Na_2O \cdot 4MoO_3$ solvent is U^{6+}.

The enthalpy of formation from the oxides, ΔH_{f-ox}^0, at 298 K was calculated for the U-pyrochlore sample (Table 4). $Ca_{1.46}U_{0.23}^{4+}U_{0.46}^{6+}Ti_{1.85}O_{7.00}$ is stable with respect to its oxides with $\Delta H_{f-ox}^0 = -123.1 \pm 3.4$ kJ/mol. Reference data were used to calculate the standard enthalpy of formation from the elements, $\Delta H_f^0 = -3610.6 \pm 4.1$ kJ/mol (Table 4). Reference data for ΔH_{f-ox}^0 $CaTiO_3$

Table 4
Thermochemical cycles for the calculation of the enthalpies of drop solution, ΔH_{ds} (kJ/mol), for the pyrochlore samples, correcting for impurities, the enthalpies of formation from the oxides, ΔH^0_{f-ox} and the standard enthalpy of formation, ΔH^0_f at 298 K

Reaction	ΔH (kJ/mol)
(1) Ce-PY$(s,298) \rightarrow [0.9748$Ce--PY $+ 0.0036CaTiO_3 + 0.0216CeO_2](sln,976)$	160.72 ± 4.48 (12)
(2) $CaTiO_3(s,298) \rightarrow CaTiO_3(sln,976)$	53.94 ± 0.64 (3)
(3) $CeO_2(s,298) \rightarrow CeO_2(sln,976)$	73.39 ± 1.65 (10)
(4) $CaCO_3(s,298) \rightarrow CaO(sln,976) + CO_2(g,976)$	120.15 ± 0.60 (6)
(5) $CO_2(g,298) \rightarrow CO_2(g,976)$	32.05[a]
(6) $CaO(s,298) + CO_2(g,298) \rightarrow CaCO_3(s,298)$	-178.80 ± 1.58[a]
(7) $TiO_2(s,298) \rightarrow TiO_2(sln,976)$	58.92 ± 0.82 (16)
(8) $Ca(s,298) + 1/2O_2(g,298) \rightarrow CaO(s,298)$	-635.09 ± 0.88[a]
(9) $Ce(s,298) + O_2(g,298) \rightarrow CeO_2(s,298)$	-1088.68 ± 1.46[a]
(10) $Ti(s,298) + O_2(g,298) \rightarrow TiO_2(s,298)$	-944.75 ± 1.26[a]
(11) $CaO(s,298) + TiO_2(s,298) \rightarrow CaTiO_3(s,298)$	-80.8 ± 1.7[a]
(12) $Gd_2Ti_2O_7(s,298) \rightarrow [Gd_2O_3 + 2TiO_2](sln,976)$	82.71 ± 2.11 (12)
(13) $Gd_2O_3(s,298) \rightarrow Gd_2O_3(sln,976)$	-148.54 ± 1.60 (10)
(14) $2Gd(s,298) + 3/2O_2(g,298) \rightarrow Gd_2O_3(s,298)$	-1819.62 ± 3.60[a]
(15) U-PY$(s,298) \rightarrow [0.577$U-PY $+ 0.423TiO_2](sln,976)$	66.85 ± 1.83 (11)
(16) $UO_{2.08}(s,298) \rightarrow [0.92UO_2 + 0.08UO_3](sln,976)$	-124.63 ± 2.30 (11)
(17) γ-$UO_3(s,298) \rightarrow \gamma$-$UO_3(sln,976)$	9.49 ± 1.53 (2)
(18) $1/2O_2(g,298) \rightarrow 1/2O_2(g,976)$	9.97[a]
(19) $U(s,298) + O_2(g,298) \rightarrow UO_2(s,298)$	-1084.91 ± 1.00[a]
(20) $U(s,298) + 3/2O_2(g,298) \rightarrow UO_3(s,298)$	-1223.80 ± 0.80[a]
Cycle for calculating the ΔH_{ds} of Ce-pyrochlore correcting for impurities	
(21) $Ca_{0.93}CeTi_{2.035}O_7(s,298) \rightarrow [0.93CaO + CeO_2 + 2.035TiO_2]$ $(sln,976)$	
$[\Delta H(1) - 0.0036\Delta H(2) - 0.0216\Delta H(3)]/0.9748$	163.05 ± 4.48
Cycle for calculating the ΔH_{ds} of CaO	
(22) $CaO(s,298) \rightarrow CaO$ $(sln,976)$	
$\Delta H(4) - \Delta H(5) + \Delta H(6)$	-90.70 ± 1.69
Cycle for calculating the ΔH^0_{f-ox} of Ce-pyrochlore	
(23) $[0.93CaO + CeO_2 + 2.035TiO_2](s,298) \rightarrow Ca_{0.93}CeTi_{2.035}O_7(s,298)$	
$-\Delta H(21) + \Delta H(3) + 2.035\Delta H(7) + 0.93\Delta H(22)$	-54.1 ± 5.2
Cycle for calculating the ΔH^0_f of Ce-pyrochlore	
(24) $[0.93Ca + Ce + 2.035Ti](s,298) + 7/2O_2(g,298) \rightarrow Ca_{0.93}CeTi_{2.035}O_7(s,298)$	
$\Delta H(23) + 0.93\Delta H(8) + 2.035\Delta H(9) + 0.93\Delta H(10)$	-3656.0 ± 5.6
Cycle for calculating the $\Delta H^0_{f-pv+ox}$ of Ce-pyrochlore	
(25) $[0.93CaTiO_3 + CeO_2 + 1.11TiO_2](s,298) \rightarrow Ca_{0.93}CeTi_{2.035}O_7(s,298)$	
$\Delta H(23) - 0.93\Delta H(11)$	$+21.0 \pm 5.5$
Cycle for calculating the ΔH^0_{f-ox} of Gd-pyrochlore	
(26) $[Gd_2O_3 + 2TiO_2](s,298) \rightarrow Gd_2Ti_2O_7(s,298)$	
$-\Delta H(12) + \Delta H(13) + \Delta H(7)$	-113.4 ± 2.8
Cycle for calculating the ΔH^0_f of Gd-pyrochlore	
(27) $[2Gd + 2Ti](s,298) + 7/2O_2(g,298) \rightarrow Gd_2Ti_2O_7(s,298)$	
$\Delta H(26) + \Delta H(14) + 2\Delta H(10)$	-3822.5 ± 4.9
Cycle for calculating the ΔH_{ds} of U-pyrochlore correcting for impurities	
(28) $Ca_{1.46}U_{0.69}Ti_{1.85}O_7(s,298) \rightarrow [1.46CaO + 0.69UO_3 + 1.85TiO_2](sln,976)$	
$[\Delta H(15) - 0.423\Delta H(7)]/0.577$	72.66 ± 1.91
Cycle for calculating the ΔH_{ds} of $UO_{2.08}$ correcting for impurities	
(29) $UO_2(s,298) + 1/2O_2(g,976) \rightarrow UO_3(sln,976)$	
$[\Delta H(16) - 0.08\Delta H(17)]/0.92$	-136.29 ± 2.34
Cycle for calculating the $\Delta H_{oxidation}$ of UO_2 to UO_3	
(30) $UO_2(s,298) + 1/2O_2(g,298)UO_3(s,298)$	
$\Delta H(29) - \Delta H(17) + \Delta H(18)$	-135.9 ± 2.8

Table 4 (*continued*)

Reaction	ΔH (kJ/mol)
Reference cycle for calculating the $\Delta H_{oxidation}$ of UO_2 to UO_3 (31) $UO_2(s,298) + 1/2\,O_2(g,298) \rightarrow UO_3(s,298)$ $-\Delta H(19) + \Delta H$ (20)	-138.8 ± 1.3
Cycle for calculating the ΔH^0_{f-ox} of U-pyrochlore (32) $[1.46CaO + 0.23UO_2 + 0.46UO_3 + 1.85TiO_2](s,298) \rightarrow Ca_{1.46}U^{+4}_{0.23}U^{+6}_{0.46}Ti_{1.85}O_7(s,298)$ $-\Delta H(28) + 0.23\Delta H(29) + 0.46\Delta H(17) + 1.85\Delta H(7) + 1.46\Delta H(22)$	-123.1 ± 3.4
Cycle for calculating the ΔH^0_f of U-pyrochlore (33) $[1.46Ca + 0.23U^{+4} + 0.46U^{+6} + 1.85Ti](s,298) + 7/2\,O_2(g,298)$ $\rightarrow Ca_{1.46}U^{+4}_{0.23}U^{+6}_{0.46}Ti_{1.85}O_7(s,298)$ $\Delta H(32) + 1.46\Delta H(8) + 0.23\Delta H(19) + 0.46\Delta H(20) + 1.85\Delta H(10)$	-3610.6 ± 4.1
Cycle for calculating the $\Delta H^0_{f-pv+ox}$ of U-pyrochlore (34) $[1.46CaTiO_3 + 0.23UO_2 + 0.46UO_3 + 0.39TiO_2](s,298) \rightarrow Ca_{1.46}U^{+4}_{0.23}U^{+6}_{0.46}Ti_{1.85}O_7(s,298)$ $\Delta H(32) - 1.46\Delta H(11)$	-5.1 ± 4.0

The reaction enthalpies are ΔH_{ds} in $3Na_2O \cdot 4MoO_3$ at 976 K. Number in parentheses is the number of experiments. The error is propagated assuming linear combinations of independent variables.

[a] Calculated using reference data from Robie and Hemingway, 1995 [52].

were used to calculate, $\Delta H^0_{f-pv+ox}$, the enthalpy of formation with respect to a perovskite plus oxide assemblage (Table 4). U-pyrochlore is energetically marginally stable relative to the perovskite assemblage with $\Delta H^0_{f-pv+ox} = -5.1 \pm 4.0$ kJ/mol. This reaction assumes that all of the Ca comes from a perovskite phase and, consequently, refers to nearly 1.5 mol $CaTiO_3$ because of the excess Ca in the U-pyrochlore sample.

7. Discussion

7.1. The role of configurational entropy in non-stoichiometric pyrochlore

Both Ca-bearing pyrochlores studied contain significant cation disorder as inferred from their non-stoichiometry. Applying the Boltzmann equation [6], assuming random, independent mixing on the A- and B-sites given the nominal pyrochlore stoichiometry $A_2B_2O_7$, the configurational entropy, S_{conf}, was calculated (Table 5). The Ce-pyrochlore sample (Ce-PY) had 0.93Ca, 0.04Ti, 1.00Ce and 0.03 cation vacancies distributed over two A-sites resulting in a S_{conf} value of 14.0 J/mol K. The U-pyrochlore sample (U-PY) had mixing on both the A- and B-sites with 1.46Ca, $0.23U^{4+}$ and $0.31U^{6+}$ distributed randomly over the two A-sites and 1.85Ti and $0.15U^{6+}$ distributed randomly over the two B-sites. This resulted in a S_{conf} value of 17.2 J/mol K. The primary assumption underlying these calculations, that of random, independent mixing, likely overestimates the S_{conf} contribution. Thus, the values presented here are upper limits for S_{conf}.

A summary of measured and calculated thermodynamic data is presented in Table 6. Estimated vibrational S^0 values were calculated by averaging the S^0 contributions from an oxide assemblage and a perovskite plus oxide assemblage. The estimated values were added to the calculated S_{conf} for an estimate of the S^0_{total}. For the $Gd_2Ti_2O_7$ (Gd-PY) sample there was no

Table 5
Configurational entropy, S_{conf} (J/mol K), for the Ce-PY and U-PY phases[a]

$Ca_{1.46}U^{4+}_{0.23}U^{6+}_{0.46}Ti_{1.85}O_{7.00}$
Cation disorder on the A-sites
$S_{conf} = k[2N_A \ln 2N_A - 1.46N_A \ln 1.46N_A - 0.23N_A \ln 0.23N_A - 0.31N_A \ln 0.31N_A] = 12.76$
Cation disorder on the B-sites
$S_{conf} = k[2N_A \ln 2N_A - 0.15N_A \ln 0.15N_A - 1.85N_A \ln 1.85N_A] = 4.43$
Total $S_{conf} = 17.2$ J/mol K
$Ca_{0.93}Ce_{1.00}Ti_{2.04}O_{7.00}$
Cation + vacancy disorder on the A-sites
$S_{conf} = k[2N_A \ln 2N_A - 0.93N_A \ln 0.93N_A - N_A \ln N_A - 0.04N_A \ln 0.04N_A - 0.03N_A \ln 0.03N_A] = 14.0$ J/mol K

[a] Calculations assume random mixing and, therefore, represent an upper limit. The Sterling approximation is applied to $S_{conf} = k \ln \Omega$, the Boltzmann equation, where k is Boltzmann's constant and Ω is the number of possible complexions.

Table 6
Enthalpy, estimated entropy and Gibbs energy of formation from the elements, oxides and a perovskite + oxide assemblage for $Ca_{0.93}Ce_{1.00}Ti_{2.04}O_{7.00}$ (Ce-PY), $Ca_{1.46}U^{4+}_{0.23}U^{6+}_{0.46}Ti_{1.85}O_{7.00}$ (U-PY) and $Gd_2Ti_2O_7$ (Gd-PY)

	ΔH^0_f (kJ/mol)	$S^0_{total} = S^0$ (J/mol K)[a] + S_{conf}	ΔG^0_f (kJ/mol)
Ce-PY	-3656.0 ± 5.6	$202.82 + 14.03 = 216.85$	-3455.7 ± 5.6
U-PY	-3610.6 ± 4.1	$215.66 + 17.19 = 232.85$	-3420.6 ± 4.1
Gd-PY	-3822.5 ± 4.9	$252.46 + 0 = 252.46$	-3641.0 ± 4.9
	ΔH^0_{f-ox} (kJ/mol)	ΔS^0_{f-ox} (J/mol K)	ΔG^0_{f-ox} (kJ/mol)
Ce-PY	-54.1 ± 5.2	16.42	-59.0 ± 5.2
U-PY	-123.1 ± 3.4	20.91	-129.3 ± 3.5
Gd-PY	-113.4 ± 2.8	0	-113.3 ± 2.8
	$\Delta H^0_{f-pv+ox}$ (kJ/mol)	$\Delta S^0_{f-pv+ox}$ (J/mol K)	$\Delta G^0_{f-pv+ox}$ (kJ/mol)
Ce-PY	$+21.0 \pm 5.5$	11.64	$+17.5 \pm 5.5$
U-PY	-5.1 ± 4.0	13.44	-9.1 ± 4.0
Gd-PY	–	–	–

[a] Neumann-Kopf rule: average of $\Sigma S^0_{f-ox} + \Sigma S^0_{f-pv+ox}$.

configurational entropy term and the estimated S^0_{total} was simply a sum of the S^0 for the oxides. The free energies, ΔG^0_f, were calculated using

$$\Delta G = \Delta H - T\Delta S. \quad (4)$$

Standard free energies, ΔG^0_f as well as free energies of formation from an oxide phase assemblage, ΔG^0_{f-ox} and a perovskite plus oxide assemblage, $\Delta G^0_{f-pv+ox}$ were calculated (Table 6). Reference data for the elements and oxides were used in these calculations [52]. With the exception of $\Delta G^0_{f-pv+ox}$ for Ce-PY, all values are negative indicating that the phases are stable at 298 K.

The Ce-PY sample is entropy stabilized with respect to a perovskite plus oxide assemblage. Thus, it is predicted to be thermodynamically unstable below a certain temperature. Using the measured value for $\Delta H^0_{f-pv+ox}$ and the estimated ΔS^0_{pv+ox}, T_{eq} was calculated such that $\Delta H^0_{f-pv+ox} = T_{eq}\Delta S^0_{pv+ox}$. A temperature range for T_{eq} was calculated by considering the error on the $\Delta H^0_{f-pv+ox}$ value for Ce-PY: $T_{eq} = 1788 \pm 463$ K. While the uncertainty in this calculation is large, the calculated T_{eq} is consistent, within error, to the observed optimum synthesis temperature, T_{syn}, of 1475 K.

7.2. Comparison to previously predicted Gibbs energy values

The estimated Gibbs energy of formation values presented by Xu and Wang [29] for Ce-PY and U-PY are inconsistent with the ΔG^0_f values calculated using data derived in this study. Their predicted $\Delta G^0_{f-pv+ox}$ for U-PY of -5 kJ/mol is, within error, equal to the value reported here of -9.1 ± 4.0 kJ/mol if one assigns a conservative error to their value of 2 kJ/mol. Their model predicted a negative $\Delta G^0_{f-pv+ox}$ for Ce-PY (-8 kJ/mol). This value is approximately 25 kJ/mol more exothermic than $\Delta G^0_{f-pv+ox}$ calculated using measured enthalpy data. Any direct comparison between their predicted values and the measured data is problematic as their model refers to stoichiometric compounds and the Ce-PY and U-PY samples are non-stoichiometric. The usefulness of a linear free energy model for a system prone to non-stoichiometry that is typically compensated by cation and/or anion vacancies may be limited.

7.3. Trends in enthalpies of Ca-bearing pyrochlore and zirconolite and the predicted enthalpy of formation for $CaPuTi_2O_7$

Plotting the ΔH^0_{f-ox} for $CaMTi_2O_7$, where M = U, Hf, Zr, Ce, as a function of the ionic potential (Z/r, where Z = weighted average cation charge and r = weighted average ionic radius) of the M-site cation (weighted by occupancy) revealed a potential problem with the previously reported hafnolite data (Fig. 6). The ΔH^0_{f-ox} for Ce-PY, U-PY and zirconolite are approximately linear with ionic potential. The hafnolite value that was determined in a previous study using lead borate as the solvent is significantly more exothermic than a linear model would predict (Fig. 6, open diamonds). In the case of complex oxides, enthalpy trends are not necessarily linear [57]. As discussed in Section 7.2, the usefulness of a linear model in the prediction of thermodynamic properties of materials prone to non-stoichiometry may be limited. In addition, the assumption that the energy associated with the transformation from zirconolite to pyrochlore is negligible may be in error (see Section 1). This assumption lends validity to plotting both structure types on one graph. However, given the relative importance of the hafnolite data to waste form energetics and the reported dissolution difficulties in $2PbO \cdot B_2O_3$, the solvent used in the previ-

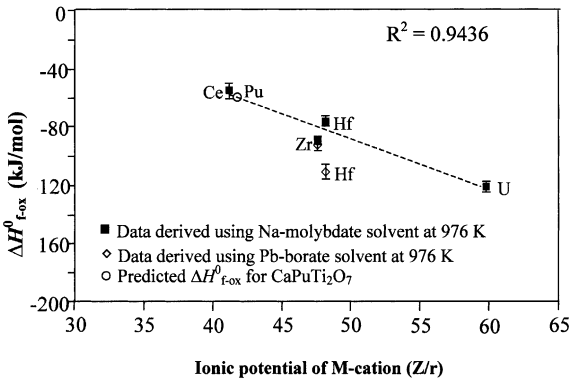

Fig. 6. Enthalpy of formation from the oxides for the $CaMTi_2O_7$ pyrochlore and zirconolite samples. Data derived using two different solvents is shown. The linear trend is fit using only the data derived using $3Na_2O \cdot 4MoO_3$ as the solvent. Error bars represent two standard deviations of the mean.

ous studies, verification of the accuracy of ΔH_f^0 for $CaHfTi_2O_7$ was deemed necessary.

A preliminary investigation (details of which will be reported elsewhere) using $3Na_2O \cdot 4MoO_3$ solvent at 976 K and the identical hafnolite sample used in the previous studies indicated that ΔH_{f-ox}^0 for $CaHfTi_2O_7$ was approximately -78 ± 3 kJ/mol. This is 32 kJ/mol more endothermic than previously reported. The new value is consistent with the linear trend proposed in Fig. 6. Cross checking the ΔH_{f-ox} for $CaZrTi_2O_7$ using $3Na_2O \cdot 4MoO_3$ solvent indicated that the previously reported value, -88.6 ± 4.5 kJ/mol, was accurate. Clearly, a detailed investigation of the formation enthalpy of hafnolite is warranted. In the meantime, a model of waste form stability using the measured data in this study and the preliminary data for hafnolite was proposed so that the most conservative estimates would be made.

The data derived from $3Na_2O \cdot 4MoO_3$ was used to fit a linear trend that accounts for approximately 94% of the variation in the data (Fig. 6). This trend is described by the following formula:

$$\Delta H_{f-ox}^0 = -3.4312(Z/r) + 83.043. \quad (5)$$

Eq. (5) was used to calculate ΔH_{f-ox}^0 for $CaPuTi_2O_7 = -60 \pm 6$ kJ/mol. Using reference data for ΔH_{f-ox}^0 for $CaTiO_3$, $\Delta H_{f-pv+ox}^0$ for $CaPuTi_2O_7$ was calculated: $+21 \pm 6$ kJ/mol. Using standard reference data [52,58] the standard enthalpy of formation from the elements, $\Delta H_f^0 = -3640 \pm 6$ kJ/mol, was calculated. These estimates can not account for possible non-stoichiometry in the $CaPuTi_2O_7$ sample, and, consequently, represent only first approximations.

7.4. Calculation of the stability field for the proposed waste form

All of the materials studied were stable with respect to an oxide phase assemblage. However, with respect to a perovskite plus oxide assemblage ($CaTiO_3 + MO_2 + TiO_2 \rightarrow CaMTi_2O_7$, where M = U, Pu, Hf) a significant metastability region was found due to the positive enthalpies of formation, $\Delta H_{f-pv+ox}^0$, for $CaPuTi_2O_7$ and

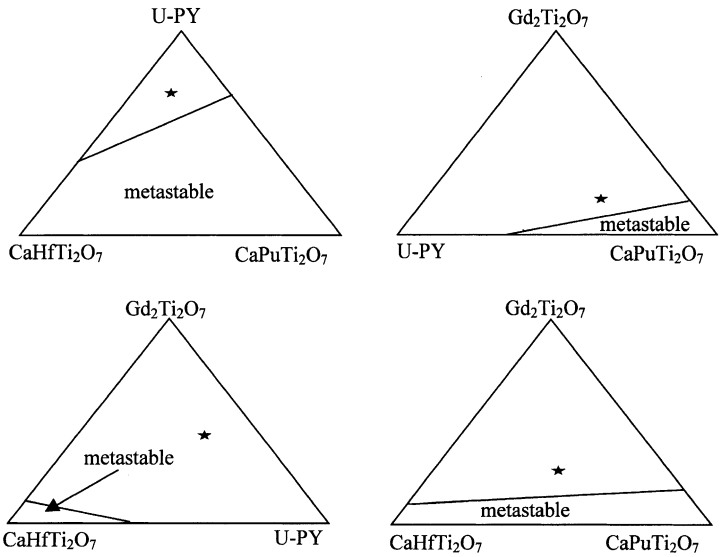

Fig. 7. Calculated metastability fields for the proposed waste form for excess weapons plutonium. Calculations assumed ideal mixing of end-members and ignored possible intermediate compound formation. ★ indicates the proposed baseline composition with respect to Gd_2O_3, HfO_2, UO_2 and PuO_2. The metastability fields as defined by data derived using $3Na_2O \cdot 4MoO_3$ solvent are shown.

$CaHfTi_2O_7$. This indicates that decomposition of some of the waste form components to the less chemically durable perovskite assemblage is thermodynamically possible.

The baseline waste form ceramic consists of (wt%) CaO – 10.0; HfO_2 – 10.6; TiO_2 – 35.9; Gd_2O_3 – 7.9; UO_2– 23.7 and PuO_2 – 11.9 [59]. Converting to mole fraction this gives a baseline composition: 0.25Hf-zirconolite + 0.11Gd-titanate pyrochlore + 0.43U-pyrochlore + 0.21 Pu-pyrochlore. Using these mole fractions, data from Table 6 and the estimated Gibbs formation energy for Pu-pyrochlore, the $\Delta G^0_{f-pv+ox}$ value for the baseline ceramic was estimated to be -9.7 ± 4.3 kJ/mol. Thus, the baseline waste form composition is thermodynamically stable with respect to perovskite + oxides.

The metastability fields in the pseudo-quaternary phase diagram representing the proposed waste form were calculated using the estimated Gibbs energies for $Gd_2Ti_2O_7$, $Ca_{1.46}U^{4+}_{0.23}U^{6+}_{0.46}Ti_{1.85}O_{7.00}$ (U-PY), $CaHfTi_2O_7$ and the estimated value for $CaPuTi_2O_7$ (Fig. 7). These calculations assume ideal mixing of the end-members, they do not account for changes in structure, nor do they account for additional stability due to configurational entropy. In this manner, the most conservative estimate of the stability regions was reached. The baseline waste form composition with respect to Gd_2O_3, HfO_2, UO_2 and PuO_2 was projected onto each face of the quaternary diagram for comparison. Significant metastability fields were defined (Fig. 7). However, the proposed waste form composition lies in the stable regions of the phase diagrams.

8. Conclusions

The three pyrochlore samples studied, $Ca_{0.93}Ce_{1.00}Ti_{2.04}O_{7.00}$, $Ca_{1.46}U^{4+}_{0.23}U^{6+}_{0.46}Ti_{1.85}O_{7.00}$ and $Gd_2Ti_2O_7$ were stable with respect to their oxide phase assemblages with ΔH^0_{f-ox} values (kJ/mol) of -54.1 ± 5.2, -123.1 ± 3.4 and -113.4 ± 2.8, respectively. The U-PY sample was also stable with respect to a perovskite plus oxide phase assemblage with $\Delta H^0_{f-pv+ox} = -5.1 \pm 4.0$ kJ/mol. The Ce-PY sample was found to be metastable with $\Delta H^0_{f-pv+ox} = +21.0 \pm 5.5$ kJ/mol, thus, Ce-PY is entropy stabilized. The previously reported ΔH^0_f for $CaHfTi_2O_7$ was shown to be in error by approximately 32 kJ/mol. A detailed investigation of this material is underway. A plot of the Ca-bearing samples revealed an approximately linear trend of H^0_{f-ox} with ionic potential of the M-site cations. As the ionic potential increases, the materials become more exothermic. These data were used to predict ΔH^0_{f-ox} for $CaPuTi_2O_7$ of -60 ± 6 kJ/mol. As enthalpy trends in complex oxides are not always linear [57], extrapolating beyond the measured data set to predict ΔH^0_{f-ox} for other actinide pyrochlores is not supported. A significant metastability field was calculated for the proposed waste form. However, the waste form baseline composition falls in the stable regions of the phase diagrams.

Acknowledgements

The authors would like to thank H. Xu for the synchrotron X-ray data and Rietveld analysis; A. Risbud and J. Majzlan for their assistance in calorimetry. Financial support was provided by Lawrence Livermore National Laboratory, the Department of Energy EMSP grant number 60118 and grant number DE-FG07-97ER45673, the University of California at Davis and by the Office of Basic Energy Sciences, DOE grant (R.C. Ewing) DE-FG02-97ER45656. Portions of this research were carried out at the Stanford Synchrotron Radiation Laboratory, a national user facility operated by Stanford University on behalf of the US Department of Energy, Office of Basic Energy Sciences.

References

[1] Record of decision for the storage and disposition of weapons-usable fissile materials, Final Programmatic Environmental Impact Statement, January 14, 1997, US Department of Energy, Washington, DC, 1997.
[2] A. Jostons, L. Vance, B. Ebbinghaus, in: Proceedings of the International Conference on Future Nuclear Systems, Global 99, Jackson Hole, WY (American Nuclear Society CDROM, 1999).
[3] R.L. Putnam, A. Navrotsky, B.F. Woodfield, J. Boerio-Goates, J.L. Shapiro, J. Chem. Therm. 31 (1999) 229.
[4] B.F. Woodfield, J. Boerio-Goates, J.L. Shapiro, R.L. Putnam, A. Navrotsky, J. Chem. Therm. 31 (1999) 245.
[5] R.L. Putnam, A. Navrotsky, B.F. Woodfield, R. Stevens, J.L. Shapiro, J. Boerio-Goates, Materials Research Society Symposium Proceedings, 1998.
[6] D.R. Gaskell, in: Introduction to the Thermodynamics of Materials, 3rd Ed., Taylor and Francis, Washington, DC, 1995, p. 568.
[7] F.D. Bloss, in: Crystallography and Crystal Chemistry, 2nd Ed., Mineralogical Society of America, Washington, DC, 1994, p. 545.
[8] F.W. Clinard Jr., D.E. Peterson, D.L. Rohr, L.W. Hobbs, J. Nucl. Mater. 126 (1984) 245.
[9] S.E. Kessen, W.J. Sinclair, A.E. Ringwood, Nucl. Chem. Waste Manage. 4 (1983) 259.
[10] H.J. Rossell, Abstracts Crystal XII, 12th Meeting of Crystallographers in Australia, 30 January–2 February, 1980, p. 242.
[11] H.J. Rossell, Nature (London) 282 (1980) 282.
[12] T.J. White, R.L. Segall, P.S. Turner, Agnew. Chem. Int. Ed. Engl. 24 (1985) 357.
[13] F.J. Ryerson, J. Am. Ceram. Soc. 67 (1984) 75.
[14] P.E.D. Morgan, T.M. Shaw, E.A. Pugar, Nuclear waste management, in: G.G. Wicks, W.A. Ross (Eds.), Advanced Ceramics, vol. 8, American Ceramic Society, Columbus, OH, 1984, p. 209.

[15] B.M. Gatehouse, I.E. Grey, R.J. Hill, H.J. Rossell, Acta Crystallogr. B 37 (1981) 306.
[16] F. Mazzi, R. Munno, Am. Mineral. 68 (1983) 262.
[17] E.R. Vance, B.D. Begg, R.A. Day, C.J. Ball, Mater. Res. Soc. Symp. Proc. 353 (1995) 767.
[18] E.R. Vance, C.J. Ball, R.A. Day, K.L. Smith, M.G. Blackford, B.D. Begg, P.J. Angel, J. Alloys Compd. 213&214 (1994) 406.
[19] E.R. Vance, MRS Bull. XIX (1994) 28.
[20] E.R. Vance, A. Jostons, M.W.A. Stewart, R.A. Day, B.D. Begg, M.J. Hambley, K.P. Hart, B.B. Ebbinghaus, Plutonium Future – The Science, Los Alamos National Laboratory, 1997, p. 19.
[21] E.R. Vance, K.P. Hart, R.A. Day, M.L. Carter, M. Hambley, M.G. Blackford, B.D. Begg, in: W.J. Gray, I.R. Triay (Eds.), Scientific Basis for Nuclear Waste Management, vol. 20, 1997, p. 341.
[22] E.R. Vance, D.K. Agnawal, Nucl. Chem. Waste Manage. 3 (1982) 229.
[23] B.D. Begg, E.R. Vance, R.A. Day, M. Hambley, S.D. Conradson, in: W.J. Gray, I.R. Triay (Eds.), Scientific Basis for Nuclear Waste Management, vol. 20, 1997, p. 325.
[24] E.R. Vance, M.L. Carter, B.D. Begg, R.A. Day, S.H.F. Leung, in: R.W. Smith, D.W. Shoesmith (Eds.), Scientific Basis for Nuclear Waste Management, vol. 23, 2000, p. 333.
[25] P.E. Fielding, T.J. White, J. Mater. Res. 2&3 (1987) 387.
[26] A. Aronson, J. Nucl. Mater. 107 (1982) 343.
[27] W.J. Weber, J.W. Wald, Hj. Matzke, in: C.M. Jantzen, J.A. Stone, R.C. Ewing (Eds.), Scientific Basis for Nuclear Waste Management, vol. VIII, 1985, p. 679.
[28] F.W. Clinard, L.W. Hobbs, C.C. Land, D.E. Peterson, D.L. Rohr, R.B. Roof, J. Nucl. Mater. 105 (1982) 248.
[29] H. Xu, Y. Wang, J. Nucl. Mater. 275 (1999) 216.
[30] D.A. Sverjensky, P.A. Molling, Nature 358 (1992) 310.
[31] L.P. Hammett, Physical Organic Chemistry, McGill-Hill, New York, 1970.
[32] E.C. Buck, D.B. Chamberlain, R. Giere, in: David Wronkiewicz (Ed.), Scientific Basis for Nuclear Waste Management XXII, vol. 556, 1999, p. 19.
[33] A. Navrotsky, Phys. Chem. Miner. 2 (1977) 89.
[34] A. Navrotsky, Phys. Chem. Miner. 24 (1997) 22.
[35] A.C. Larson, R.B. von Dreele, GSAS – general structure analysis system, LANSCE, MS-H805, Los Alamos, NM, 1994.
[36] RIQAS software from Materials Data, Inc.
[37] G.N. George, I.F. Pickering, http://ssrl.slac.stanford.edu/exafspak.html, Stanford Synchrotron Radiation Laboratory, Stanford, CA, 1995.
[38] S.I. Zabinsky, J.J. Rehr, A. Ankudinov, R.C. Albers, M.J. Eller, Phys. Rev. B 52 (1995) 2995.
[39] L.R. Morss, Mater. Res. Soc. Symp. Proc. 257 (1992) 275.
[40] M.A. Subramanian, A.W. Sleight, in: K.A. Gschneider Jr., L. Eyring (Eds.), Handbook on the Physics and Chemistry of Rare Earths, vol. 16, Elsevier Science, Amsterdam, 1993, p. 225.
[41] J.I. Goldstein, D.E. Newberry, P. Echlin, D.C. Joy, A.D. Romig Jr., C.E. Lyman, C. Fiori, E. Lifshin, in: Scanning Electron Microscopy and X-ray Microanalysis, 2nd Ed., Plenum, New York, 1992, p. 820.
[42] W.A. Deer, R.A. Howie, J. Zussman, in: An Introduction to the Rock Forming Minerals, Longman, New York, 1966, p. 528.
[43] S.X. Wang, L.M. Wang, R.C. Ewing, K.V. Govidan Kutty, Mater. Res. Soc. Symp. Proc. 540 (1999) 704.
[44] S.X. Wang, L.M. Wang, R.C. Ewing, G.S. Was, G.R. Lumpkin, Nucl. Instrum. and Meth. B 148 (1999) 135.
[45] S.X. Wang, L.M. Wang, R.C. Ewing, K.V. Govidan Kutty, Nucl. Instrum. and Meth. B 169 (2000) 135.
[46] B.D. Begg, N.J. Hess, D.E. McCready, S. Thevuthasan, W.J. Weber, J. Nucl. Mater. 289 (2001) 188.
[47] F. Farges, C.W. Ponader, G. Calas, G.E. Brown, Geochim. Cosmochim. Acta 56 (1992) 4205.
[48] P.M. Bertsch, D.B. Hunter, S.R. Sutton, S. Bajt, M.L. Rivers, Environ. Sci. Technol. 28 (5) (1994) 980.
[49] L.N. Moyes, R.H. Parkman, J.M. Charnock, D.J. Vaughan, F.R. Livens, C.R. Hughes, A. Braithwaite, Environ. Sci. Technol. 34 (6) (2000) 1062.
[50] A. Navrotsky, J. Therm. Anal. Calorim. 57 (1999) 653.
[51] NBS certificate: standard reference material 720, April, 1982.
[52] R.A. Robie, B.S. Hemingway, Thermodynamic properties of minerals and related substances at 298.15 K and 1 Bar (10^5 Pascals) pressure and at higher temperatures, US Geol. Surv. Bull. 2131, Washington, DC, 1995.
[53] A. Navrotsky, O.J. Kleppa, J. Am. Ceram. Soc. 50 (1967) 626.
[54] A. Navrotsky, O.J. Kleppa, J. Inorg. Nucl. Chem. 30 (1968) 479.
[55] E.R. Vance, 2000, personal communication.
[56] S.V. Ushakov, K.B. Helean, A. Navrotsky, L. Boatner, J. Mater. Res. 16 (2001) 2623.
[57] A. Navrotsky, Ceram. Trans. 119 (2001) 137.
[58] L.B. Pankratz, US Bureau Mines Bull. 672 (1982).
[59] B.B. Ebbinghaus, R.A. von Konynenburg, E.R. Vance, A. Jostens, R.G. Anthony, D.J. Wronkiewicz, in: Proceedings of the Department of Energy Plutonium Stabilization and Immobilization Workshop, 1995, p. 253.